Appendix and dataset: Convex Hull Formulations for Linear Modeling of Energy Storage Systems

David Pozo, *Senior Member, IEEE*

***Abstract*—This document is an appendix to the IEEE PES letter *Convex Hull Formulations for Linear Modeling of Energy Storage Systems* [1]. It extends the interpretation of the convex hulls, presents a general formulation of the vertices, and elaborates on the numerical experiments conducted.**

I. Introduction

Motivated by the pursuit of finding linear representations for energy storage systems (ESS), the IEEE PES letter [1] introduces two linear polyhedra, namely **HCH-LP** and **VCH-LP**, to address the limitations of the original model **ESS-MILP**. These formulations offer the tightest convex hull representation of an ESS that consider the inclusion of binary variables to manage simultaneous charging and discharging. **HCH-LP** and **VCH-LP** are free of binary variables, being a proxy to the original formulation **ESS-MILP**.

The subsequent sections provide additional descriptions to facilitate the understanding of the feasible operation region and the decision space for the ESS in both charging and discharging modes. Furthermore, a general representation of the vertices is presented to provide a comprehensive understanding of the solution space. Finally, the numerical analysis presented in the original letter [1] is expanded upon with additional data description and further result analysis.

II. Understanding Convex Hull Formulation

The letter [1] presents an ESS model, referred to as **ESS-MILP**, which incorporates equations for the account of the backlog energy, charging and discharging power capacity rates, and minimum and maximum state of energy (SoE) limits. Additionally, non-simultaneous charging and discharging constraints are taken into account. Due to the inclusion of binary variables, the **ESS-MILP** formulation results in a set of mixed-integer linear formulations.

Based on *Observation 1* of the IEEE PES letter [1], the feasible operating region in the (p_t^c, p_t^d, e_t)-space was depicted. It was demonstrated that the charging and discharging modes correspond to nonempty polytopes within the (p_t^c, p_t^d, e_t)-space. Subsequently, two linear convex hull formulations were derived, known as the convex hull V-representation (**VCH-LP**) and the convex hull H-representation (**HCH-LP**).

Importantly, it was observed that all the vertices of the convex hull can be determined *ex-ante*, solely utilizing standard ESS parameters. This insight allows for a comprehensive understanding of the convex hull's geometry and its relation to the ESS model.

Example: Consider a 2-hour duration ESS, i.e., it can be fully charged and discharged within a 2-hour period. To simplify the analysis, efficiencies are assumed to be equal to 1. The ESS operates over a time horizon spanning several hours, and the parameter values for the ESS are provided in Table I. Figure 1 showcases the projections of the example onto the (p_t^c, e_t)-space when the ESS is in charging mode (depicted in pink) and the (p_t^d, e_t)-space when the ESS is in discharging mode (depicted in green). These projections offer insights into the behavior and characteristics of the ESS under different operating modes.

TABLE I: ESS parameters

$\underline{\mathbf{E}}$	$\overline{\mathbf{E}}$	$\overline{\mathbf{P}}^{\mathbf{c}}$	$\overline{\mathbf{P}}^{\mathbf{d}}$	$\eta^{\mathbf{c}}$	$\eta^{\mathbf{d}}$
0	2	1	1	1	1

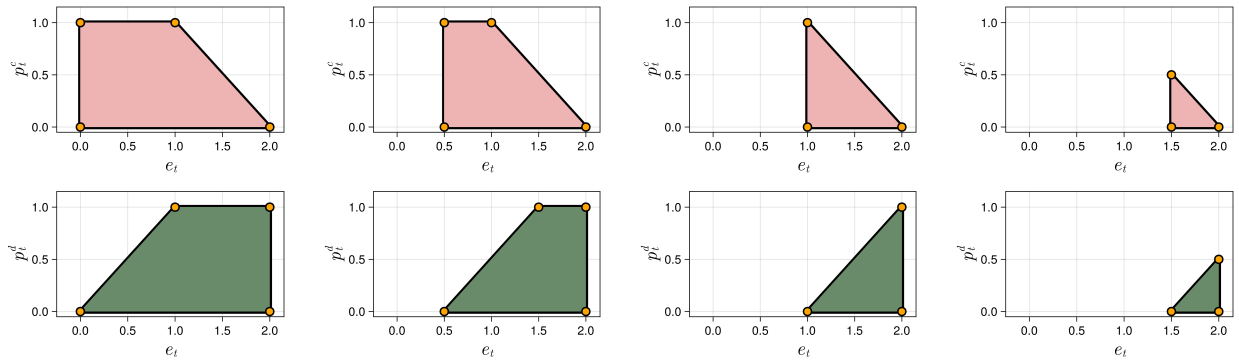

(a) $\underline{E} = 0$ (b) $\underline{E} = 0.5$ (c) $\underline{E} = 1$ (d) $\underline{E} = 1.5$

Fig. 1: Projections of the **ESS-MILP** onto the 2D (p_t^c, e_t)-space when ESS is in charging mode (in pink color), and (p_t^d, e_t)-space when ESS is in discharging mode (in green color). Each case shows the convex hull for several variations on the minimum SoE of the ESS.

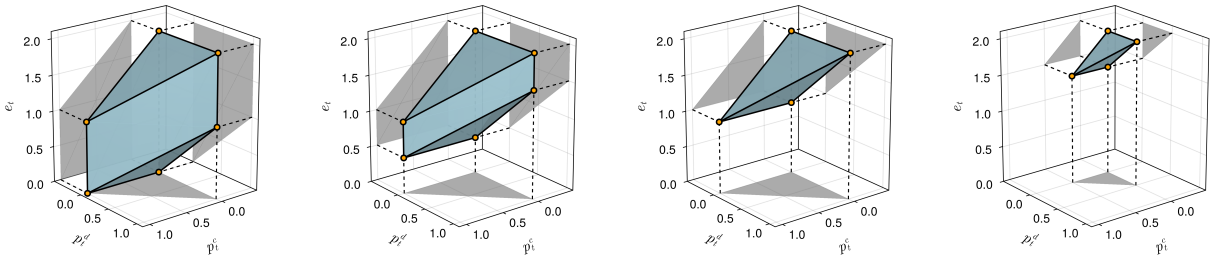

(a) $\underline{E} = 0$ (b) $\underline{E} = 0.5$ (c) $\underline{E} = 1$ (d) $\underline{E} = 1.5$

Fig. 2: Convex hull of the **ESS-MILP**. Each case shows the convex hull for several variations on the minimum SoE of the ESS.

Let us focus our attention on the top part of Figure 1. Specifically, observe that the charging capacity p_t^c does not always reach the upper limit $\overline{P}^c$ (represented by the pink region). It depends on the energy level at period t, i.e., e_t.

Consider a scenario where, at time period t, the ESS has an energy stored value of 1.5 (i.e., $e_t = 1.5$). Since the ESS capacity is 2, the maximum charging power capacity cannot be 1, but rather 0.5. It means that in 1 hour, it is only possible to charge at the power rate of 0.5. After 1 hour of charging at rate $p_t^c = 0.5$, the ESS will be full. This more stringent power rate limit can be calculated as $(\overline{E} - e_t)/\eta_c = (2 - 1.5)/1 = 0.5$. Once again, the limit $p_t^c \leq (\overline{E} - e_t)/\eta_c$ is enforced when the energy storage system (ESS) is nearing its full capacity. In this case, the charging power rate p_t^c in a single period cannot reach its technical limit of $\overline{P}^c - e_t$ due to the energy capacity constraint.

Now, let us assume that the ESS is slightly more charged, for example, $e_t = 1.9$. In this case, the maximum charging capacity is 0.1 rather than the full $\overline{P}^c$ value of 1.

On the other hand, let us consider an extreme scenario where the battery is at a very low level at time period t, such as $e_t = 0.5$. This scenario is only applicable to cases depicted in Figure 1a and 1b, where the minimum SoE is at least 0.5. When $e_t = 0.5$, there is room to charge an additional 1.5 units of energy. However, due

to the maximum charging rate limit of $\overline{P}^c$, which allows for charging at the power rate of 1 unit of energy per hour, it is not possible to fully charge the battery within a single hour (recalling that $\Delta = 1$).

Based on these observations, one can construct the feasible decision region for the charging power rate p_t^c in relation to the SoE, e_t, within the same specific time period t. It is fascinating to note that the feasible region for charging exists solely in the (p_t^c, e_t)-space and is independent of the discharging power rates p_t^d. Furthermore, it is possible to determine all the vertices of the (p_t^c,e_t) feasible region of the **ESS-MILP** formulation beforehand.

From the same Figure 1 (bottom part), similar limits can be derived for the case of discharging power rates. The feasible decision region for the discharging power rate p_t^d is represented in green color in the (p_t^d, e_t)-space. Importantly, this region is independent of the charging power rates p_t^c. Additionally, all the vertices of the (p_t^d,e_t)-region can be determined beforehand, enabling an *ex-ante* computation of these critical points.

Figure 2 showcases the convex hull for four scenarios explained above, each representing a case where the minimum storage level, $\underline{E}$ is modified. This visual representation aids in clarifying the relationship between the convex hull and the constraints imposed on the ESS storage level.

III. Universal Coordinates of the Convex Hull for any ESS

In *Observation 2*, the V-representation convex hull of the **ESS-MILP** is explicitly constructed by employing a linear convex combination of the vertices of the ESS feasible region. These vertices, denoted as $\mathbf{V}$, remain constant and are not dependent on the time period. While the IEEE PES letter [1] focuses on a specific case that is commonly encountered in actual power system applications, it may not fully capture the behavior of every ESS configuration. To provide a universal representation, the mathematical expression for $\mathbf{V}$ is given in Equation (1). The preceding section provided an explanation of how it has been determined these limits.

$$\mathbf{V} = \begin{array}{c} \begin{matrix} \hat{\mathbf{p}}^{\mathbf{c}} & \hat{\mathbf{p}}^{\mathbf{d}} & \hat{\mathbf{e}} \end{matrix} \\ \begin{bmatrix} 0 & 0 & \underline{E} \\ \min(\overline{P}^c, (1/\Delta)(\overline{E}-\underline{E})/\eta^c) & 0 & \underline{E} \\ \min(\overline{P}^c, (1/\Delta)(\overline{E}-\underline{E})/\eta^c) & 0 & \min(\overline{E},\ \overline{E}-\overline{P}^c\Delta\eta^c) \\ 0 & 0 & \overline{E} \\ 0 & \min(\overline{P}^d, (1/\Delta)(\overline{E}-\underline{E})\eta^d) & \overline{E} \\ 0 & \min(\overline{P}^d, (1/\Delta)(\overline{E}-\underline{E})\eta^d) & \max(\underline{E},\ \underline{E}+\overline{P}^d\Delta/\eta^d) \end{bmatrix} \end{array} \begin{matrix} C_1\text{-}D_4 \\ C_2 \\ C_3 \\ C_4\text{-}D_1 \\ D_2 \\ D_3 \end{matrix} \quad (1)$$

IV. Numerical Experiments

The following subsection focuses on the numerical analysis of the Set Point Tracking (SPT) problem, which serves as a representative case where complementarity between charging and discharging is typically not satisfied. The SPT problem is proposed within the context of a household with PV generation, aiming to track a power signal using a battery. During periods of excess renewable energy and a fully charged battery, the optimization model deliberately "*wastes energy by charging and discharging*" the battery (round efficiency must be less than 1). This charging and discharging behavior helps minimize the error in following the power signal when there is a surplus of PV generation and insufficient capacity to store additional energy.

The SPT problem serves as an extreme application that pushes the limits of battery operation, making it a suitable scenario for validating the adequacy of linear models and examining the utilization of binary variables. To further understand the implications of the SPT problem, a 24-hour horizon with hourly intervals is defined, and the problem was executed 100 times. Each instance was generated by randomly selecting unique battery parameters and PV profiles.

A. Data

The data used for each problem instance has been synthetically generated. It is available in [2]. 725 daily profiles for PV generation were generated from 2018

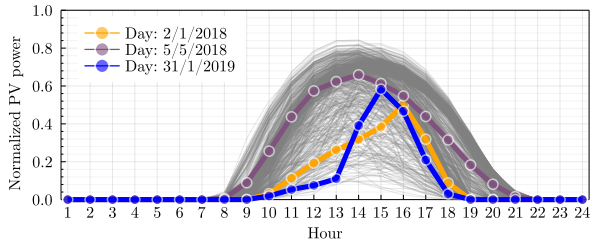

Fig. 3: Normalized RES daily profiles, 725 solar PV sited at Castilla-La Mancha region, Spain, taken from years 2018 and 2019. Three random days are represented in orange, purple, and blue for PV generation daily profiles.

and 2019 using *renewables.ninja*[1]. Fig 3 summarizes the normalized profiles for a unit-capacity power plant.

ESS parameters were randomly generated using the probabilistic values listed in Table II.

B. Simulation Tests Setup

Five formulations for modeling ESS are tested. These formulations are analyzed and compared to evaluate their effectiveness and performance in modeling and optimizing ESS operations in the SPT problem. The ESS models are the next:

- **ESS-MILP**: The original mixed-integer formulation that includes binary variables.
- **HCH-LP**: The H-representation of the convex hull.
- **VCH-LP**: The V-representation of the convex hull.
- **Simp-LP**: A simplified linear programming ESS model (*Observation 4 (i)*).
- **Relax-LP**: The original mixed-integer formulation that has relaxed the binary variables (*Observation 4 (iii)*).

All numerical experiments were executed to optimality using Gurobi 10.0.1 with default options. The implementation was performed in Julia 1.9.0 with JuMP 1.11.1 and executed on a Macbook Pro equipped with an Apple M1 chip and 16 GB of RAM.

[1]https://www.renewables.ninja/

TABLE II: ESS parameter generation

$\underline{\mathbf{E}}$	$\overline{\mathbf{E}}$	$\overline{\mathbf{P}}^{\mathbf{c}}$	$\overline{\mathbf{P}}^{\mathbf{d}}$	$\eta^{\mathbf{c}}$	$\eta^{\mathbf{d}}$
$\mathcal{U}(0,30)$	$\mathcal{U}(40,80)$	$\mathcal{U}(10,20)$	$\mathcal{U}(10,20)$	$\mathcal{U}(0.75,1)$	$\mathcal{U}(0.75,1)$

$\mathcal{U}(a,b)$ is a continuous Uniform distribution between a and b.

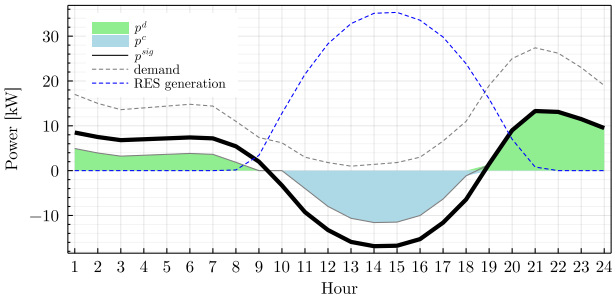

Fig. 4: Data and solution example for the SPT problem and a single instance when using **ESS-MILP** model. ESS parameters are randomly selected. The p^{sig} is built upon a deterministic demand and a random PV profile. p^c and p^d are solutions to the SPT problem.

C. Results and Analysis

Figure 4 presents the data and optimal results for a specific problem instance. The net demand, denoted as p^{sig}, is generated by subtracting the deterministic demand profile from the random PV generation profile. The black line represents the desired signal that should be followed using the available battery. The solution of charging and discharging for this particular instance is visualized in blue and green, respectively.

The comparison of the ESS models involves evaluating occurrences of simultaneous charging and discharging (determined by the condition $|p_t^c p_t^d| > 10^{-4}$) and solution time. Table III presents a summary of the results obtained from each ESS formulation.

TABLE III: Summary of numerical experiments.

ESS Formulation	$\lvert p_t^c p_t^d\rvert > 10^{-4}$ [%]	Time [ms]
ESS-MILP	0.0	5
HCH-LP	15.5	0.76
VCH-LP	15.5	1.12
Simp-LP	29.0	0.47
Relax-LP	29.5	0.73

The numerical example presented in this study effectively demonstrates the capability of the proposed convex hull formulations (**HCH-LP** and **VCH-LP**) to mitigate the occurrence of simultaneous charging and discharging actions. Both convex hulls yield the same solution, as observed in the Minkowski-Weyl theorem (Observation 4(ii)). In the context of the SPT problem, approximately

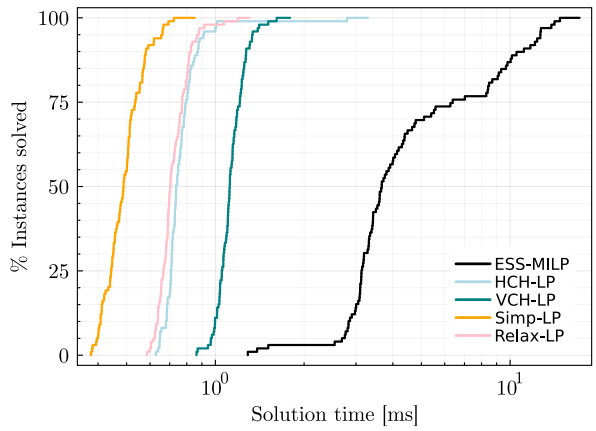

Fig. 5: Computational performance curves representing the percentage of instances solved vs. runtime for solving each of them.

15.5% of the hours exhibit simultaneous charging and discharging. However, when using a standard **Simp-LP** model for the battery, this percentage nearly doubles. It is important to note that the relaxation **Relax-LP** provides similar results to the **Simp-LP** model in terms of the lack of fulfillment of complementarity between charging and discharging actions.

Furthermore, it is essential to highlight that the linear convex hulls proposed in the IEEE PES letter [1] represent the tightest polyhedra encompassing all feasible solutions of the original **ESS-MILP** model. However, it is crucial to acknowledge that these convex hulls are not identical to the **ESS-MILP** model, thereby allowing for the possibility of simultaneous charging and discharging, as exemplified in the extreme application of the SPT problem.

The geometric representations of the convex hull and the feasible solution space of the original problem clearly illustrate that the convex hull occupies a larger decision space. Nevertheless, it is important to emphasize that the convex hulls and **ESS-MILP** models share the same vertices, confirming that the convex hulls proposed in the letter [1] constitute the tightest linear polyhedron among all the linear polyhedra approximations.

The last column of Table III represents the average resolution time for each problem instance. The **ESS-MILP** model proves more challenging to solve due to the binary variables. The **Simp-LP** model provides the fastest solution. Among the two convex formulations, **HCH-LP** outperforms **VCH-LP** in this application context, possibly due to the additional 144 decision variables, λ_{tk}, that **VCH-LP** entails. Solution time is further visualized by the performance curves. The performance curves for each ESS model have been illustrated in Figure 5. The y-axis indicates the percentage of instances resolved, while the x-axis (on a logarithmic scale) represents the cumulative time required to solve each of the 100 randomly generated instances, measured in milliseconds.

REFERENCES

[1] D. Pozo, "Convex hull formulations for linear modeling of energy storage systems," *IEEE Transactions on Power Systems*, pp. 1–4, 2023.

[2] D. Pozo, "Appendix and dataset: Convex hull formulations for linear modeling of energy storage systems." https://github.com/DavidPozo/ESS_data, 2023.